

## Video-Rate Scanning Two-Photon Excitation Fluorescence Microscopy and Ratio Imaging with Cameleons

G. Y. Fan,\* H. Fujisaki,\*<sup>#</sup> A. Miyawaki,<sup>§</sup> R.-K. Tsay,\* Roger Y. Tsien,<sup>§¶</sup> and Mark H. Ellisman\*

\*National Center for Microscopy and Imaging Research, Department of Neurosciences, School of Medicine, <sup>¶</sup>Howard Hughes Medical Institute, and <sup>§</sup>Department of Pharmacology, University of California, San Diego, California 92093 USA; and <sup>#</sup>Nikon Corporation, Tsukuba Research Laboratories, Ibaraki 300-2635, Japan

**ABSTRACT** A video-rate (30 frames/s) scanning two-photon excitation microscope has been successfully tested. The microscope, based on a Nikon RCM 8000, incorporates a femtosecond pulsed laser with wavelength tunable from 690 to 1050 nm, prechirper optics for laser pulse-width compression, resonant galvanometer for video-rate point scanning, and a pair of nonconfocal detectors for fast emission ratioing. An increase in fluorescent emission of 1.75-fold is consistently obtained with the use of the prechirper optics. The nonconfocal detectors provide another 2.25-fold increase in detection efficiency. Ratio imaging and optical sectioning can therefore be performed more efficiently without confocal optics. Faster frame rates, at 60, 120, and 240 frames/s, can be achieved with proportionally reduced scan lines per frame. Useful two-photon images can be acquired at video rate with a laser power as low as 2.7 mW at specimen with the genetically modified green fluorescent proteins. Preliminary results obtained using this system confirm that the yellow "cameleons" exhibit similar optical properties as under one-photon excitation conditions. Dynamic two-photon images of cardiac myocytes and ratio images of yellow cameleon-2.1, -3.1, and -3.1nu are also presented.

### INTRODUCTION

Two-photon excitation microscopy (TPEM) Denk et al., 1990) represents one of the most significant advances in light microscopy since the introduction of laser-scanning confocal microscopy (Carlsson et al., 1985; Åslund et al., 1998; White et al., 1987; Amos et al., 1987). In addition to providing optical sections of a thick biological specimen without physically cutting it, which is the key ability of the confocal microscopy that revolutionized three-dimensional (3D) imaging in light microscopy, TPEM also offers other attractive advantages. The simultaneous absorption of two incident photons in a two-photon excitation process allows the use of longer-wavelength photons to excite a fluorophore, as the energy of each photon needs only to be half that required to cause the transition from the ground to an excited state of the fluorophore. Thus, near infrared light, which is less harmful to living cells and generally has a better penetration in living tissues, can be used to excite UV-absorbing fluorophores in TPEM. The simultaneous absorption of two photons also means that the cross section of this quantum event depends on the square of the instantaneous intensity of the incident light. This square dependence naturally confines the absorption to where the incident light is the strongest, such as the focal point of an objective lens, thus reducing photobleaching elsewhere in the specimen. A dramatic demonstration of this effect has been given by Piston et al. (1995), who showed convinc-

ingly that photobleaching is highly localized to a narrow layer in *z*, corresponding to the focal plane, in the case of TPEM, whereas nearly uniform bleaching occurs above and below the focal plane in the case of confocal (one-photon excitation) microscopy. The lack of bleaching outside the focal plane is particularly valuable when one is accumulating a stack of optical sections or viewing a diffusible fluorophore within a thick specimen. This spatial localization affords TPEM the intrinsic 3D resolution without the necessary use of a pinhole aperture and other confocal optics as does confocal microscopy, thus simplifying the TPEM optics and improving detection efficiency, especially when the emitted light undergoes considerable scattering.

Many existing fluorophores have been tested for TPEM, including the commonly used dyes such as fluorescein and rhodamine, Ca<sup>2+</sup> indicators such as indo-1, and early versions of green fluorescent protein (GFP) (Xu and Webb, 1996; Xu et al., 1996). Two-photon excitation spectra often differ considerably in shape and peak wavelengths from a doubled-wavelength version of the one-photon excitation spectra, because the selection rules are different (Berge, 1979; Loudon, 1983). However, almost all fluorophores show the same emission spectra with either mode of excitation (Curley et al., 1992; Xu and Webb, 1996).

A new class of protein-based Ca<sup>2+</sup> indicators dubbed "cameleons" has major advantages over previous small-molecule indicators in that the cameleons are entirely genetically encoded and targetable to specific tissues and intracellular locations (Miyawaki et al., 1997). The cameleons are based on fluorescence resonance energy transfer (FRET) between donor and acceptor GFP mutants fused to calmodulin (CaM) and a CaM-binding peptide (M13), respectively. Binding of Ca<sup>2+</sup> to the CaM makes it bind the peptide, increasing the FRET between the two GFPs. Thus,

*Received for publication 3 August 1998 and in final form 8 February 1999.*

Address reprint requests to Dr. Gary Fan, National Center for Microscopy and Imaging Research, Department of Neurosciences, School of Medicine, University of California, San Diego, San Diego, CA 92093. Tel.: 619-534-5637; Fax: 619-534-7497; E-mail: gfan@ucsd.edu.

© 1999 by the Biophysical Society

0006-3495/99/05/2412/09 \$2.00

$\text{Ca}^{2+}$  increases the donor's emission and decreases the acceptor's. The ratio of intensities at their respective emission wavelengths is therefore a quantitative measure of the dynamic concentration of free  $\text{Ca}^{2+}$ . The preferred donor and acceptor GFPs are now cyan and yellow mutants, respectively, because they have the correct spectral overlap for FRET, and the cyan is much brighter and more photostable than the blue mutant previously used as a donor to green acceptors. However, cyan and yellow GFPs have not been previously tested with two-photon excitation, so it was unclear whether a wavelength could be found at which two-photon excitation could selectively excite the cyan without directly exciting the yellow as well. Such selective excitation is necessary for monitoring FRET and can be assessed by comparing the maximal ratio change from zero to saturating  $\text{Ca}^{2+}$  seen with one-photon versus two-photon excitation.

The TPEM systems so far reported typically require 1 s or longer for a single full-frame scan, but many biological processes in living cells or tissues undergo much faster changes. Scanning at normal video rate (National Television Standards Committee: 30 frames/s) is the appropriate next step in faster image rates because it allows for real-time monitoring, recording, and processing using standard video equipment. Two main methods have been demonstrated for video-rate scanning in one-photon excitation, acousto-optical deflectors, and resonant galvanometer mirrors (Tsien and Bacskai, 1995). Acousto-optical deflection is inherently ill-suited to TPEM, because the spectral bandwidth of the femtosecond laser pulses would be significantly dispersed by the acoustically generated diffraction grating. Resonant galvanometers are simple mirrors that work just as well in TPEM as in one-photon excitation and are therefore the method of choice for fast TPEM.

Systems with faster scan rate have also been reported recently, in which line excitation (Brakenhoff et al., 1996) and rotating microlens array (Bewersdorf et al., 1998) are used to achieve scan rates faster than video rate. In both implementations, an image is formed on a 2D detector.

Therefore, image quality relies on the spatial registration of the fluorescent photons, which, as pointed out by Denk and Svoboda (1997), suffer from light-scattering problems, particularly for thick tissues, due to refractive index inhomogeneities present in the tissue. Also, 2D detectors would be inconvenient for fast emission ratioing because expensive cameras would have to be duplicated and put into exact spatial registration. Any future extension to excited-state lifetime detection would be much more difficult with imaging than with nonimaging detectors.

In this paper, we report the successful test of a video-rate scanning point-excitation TPEM system that provides 30 frames/s of noninterlaced images of  $512 \times 484$  pixels. The video images can be displayed and recorded with standard NTSC equipment. Preliminary results obtained with this system, including ratio imaging with cameleons under two-photon excitation, are presented.

## MATERIALS AND METHODS

### Microscope instrument

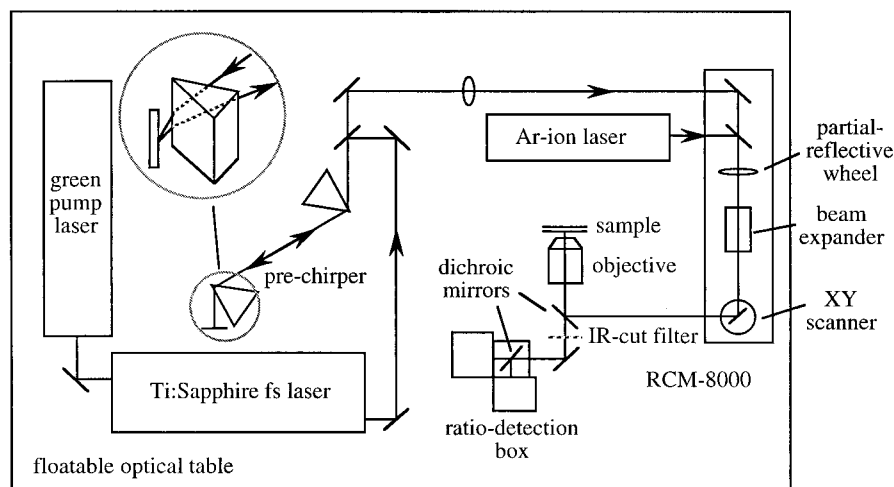
Fig. 1 shows the schematic layout of the instrument. It consists of four main components: 1) a femtosecond pulsed Ti:sapphire laser (Tsunami from Spectra Physics, Mountain View, CA), 2) a light microscope (modified Nikon RCM 8000), 3) a prechirper unit, and 4) a ratio detection box.

The Tsunami Ti:sapphire laser is optically pumped by a 5-W green laser (Millennium from Spectra Physics) and is capable of generating 100-fs pulse trains at a repetition rate of 82 MHz. The output wavelength is tunable from 690 to 1050 nm with three optical sets, each covering part of the spectrum with some overlap. The output laser beam, with an average power of 0.7–0.9 W, is vertically polarized.

### Microscope and video-rate scanner

The microscope used for this experiment is a Nikon RCM 8000 (Tsien and Bacskai, 1995). This confocal microscope incorporates a 7.875-kHz resonant galvanometer mirror for horizontal scanning. Bi-directional scanning makes the effective scan rate 15.75 kHz, which is the NTSC line scan rate. As the resonant mirror vibrates sinusoidally, the scan speed varies across each scan line, being fastest at the center and slowest at the end of each line. If the pixels were sampled at constant time intervals, the inter-pixel

FIGURE 1 Schematic set-up of the video-rate scanning two-photon excitation microscope (TPEM). The Ar-ion and the Ti:sapphire lasers are used for one- and two-photon excitations, respectively.



spacing would vary across each line, causing image distortion. To avoid this problem, sampling takes place at nonconstant time intervals, and the sampling timing is provided by detecting the position of a reference beam on a Ronchi grating that consists of 260 pairs of clear and opaque stripes of equal width. The digitized signal from one direction of the bi-directional scans is electronically reversed to provide a noninterlaced video output. Because the detectors are nonimaging, their signal amplitude is independent of the instantaneous scan velocity, assuming that bleaching and excited-state saturation are not significant during the 70–160 ns required for the beam to traverse a pixel (Tsien and Bacskai, 1995). The detector output is low-pass-filtered rather than integrated before digitization, so the nonuniform time intervals between samples do not cause any variation in the digitized values. Residual spatial nonuniformities, including optical vignetting, were found to be 1.7% from image center to corners when the system is carefully aligned, which could be further corrected by acquiring a gain-reference image (averaged over a long period of time) from a spatially uniform solution sample. Other experimental images will be divided, pixel by pixel, by this gain-reference image. Normally, a dark-level image is also acquired with the laser beam off, which will be subtracted from the experimental images before the division. As the photomultiplier tubes (PMTs) we currently use are extremely quiet, and the dark level is zero when the laser beam is off, this step is skipped.

The laser power at the specimen is controlled by a partially reflective wheel (Fig. 1) that has a gradually varying reflectivity and can be rotated to change the laser power transmitted.

An IR-cut filter, Chroma E650SP (from Chroma Technology, Brattleboro, VT) is installed below the dichroic mirror (Fig. 1), which prevents scattered and reflected excitation photons from reaching the PMT detector or the eyepieces. The IR-cut filter has a cutoff wavelength of 650 nm beyond which the transmittance is less than 0.1%.

## Prechirper

An undesirable consequence of using ultra-short laser pulses is group velocity dispersion. This is caused by the dispersive media in the optics, whose refractive index and hence the optical path length generally has a positive second derivative with respect to wavelength. The result is a chirped, or frequency-swept, pulse that has a reduced peak intensity.

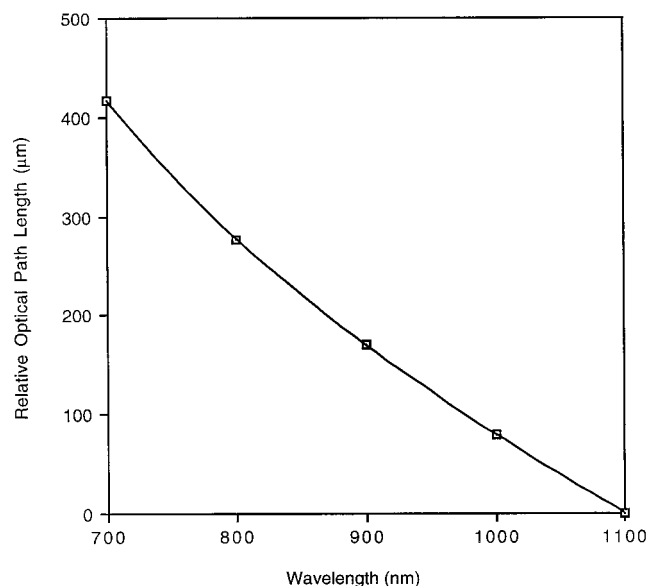


FIGURE 2 Relative optical path length in Nikon RCM 8000 microscope as a function of wavelength. The nondiminishing second derivative causes group velocity dispersion in the laser pulse train and widens the pulses and hence reduces their peak intensity.

TABLE 1 Relative optical path length ( $L$ ) and its first and second derivatives ( $dL/d\lambda$  and  $d^2L/d\lambda^2$ ) at different wavelengths ( $\lambda$ ) for Nikon RCM 8000 microscope

$\lambda$ (nm)	$L$ ( $\mu\text{m}$ )	$dL/d\lambda$ (dimensionless)	$d^2L/d\lambda^2$ ( $\text{nm}^{-1}$ )
700	415.8	-1610	2.56
800	276.9	-1200	1.55
900	169.6	-966	0.854
1000	79.9	-840	0.464
1100	0	-761	0.384

The dispersion properties of some microscope objective lenses have been determined and have been shown to cause substantial pulse widening if left uncompensated (Guild et al., 1997). The optical path length of the Nikon RCM 8000 with a 40 $\times$  water-immersion objective lens is shown in Fig. 2 as a function of wavelength. Its first and second derivatives are negative and positive, respectively (Table 1), as is typical for commonly used optical glasses. The first derivative merely reduces the group velocity of the pulses, but the nonzero second derivative causes dispersion and widens the pulses. As two-photon excitation depends quadratically on the peak intensity of the pulses, it is highly desirable to restore the pulses to a width as short as possible to maintain a good temporal concentration of the laser power on the specimen. As demonstrated by Fork et al. (1984), negative dispersion can be created using prism pairs, as shown in Fig. 1. A similar implementation has also been reported by Brakenhoff et al. (1995).

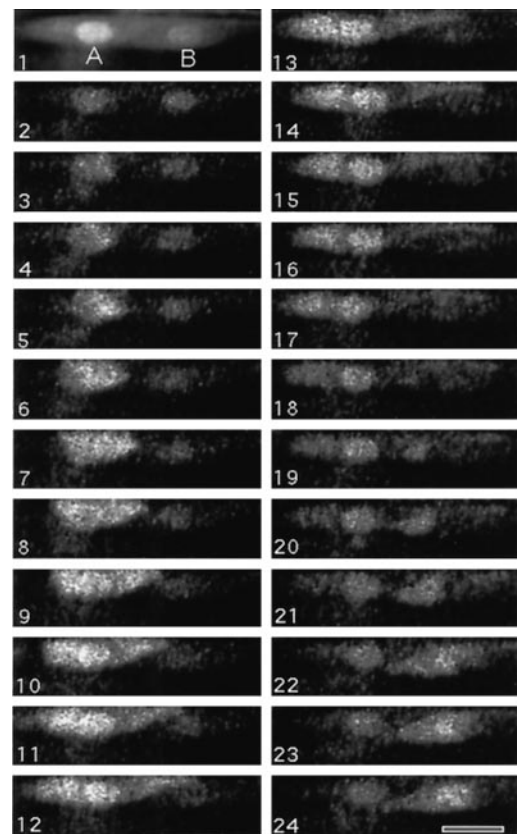
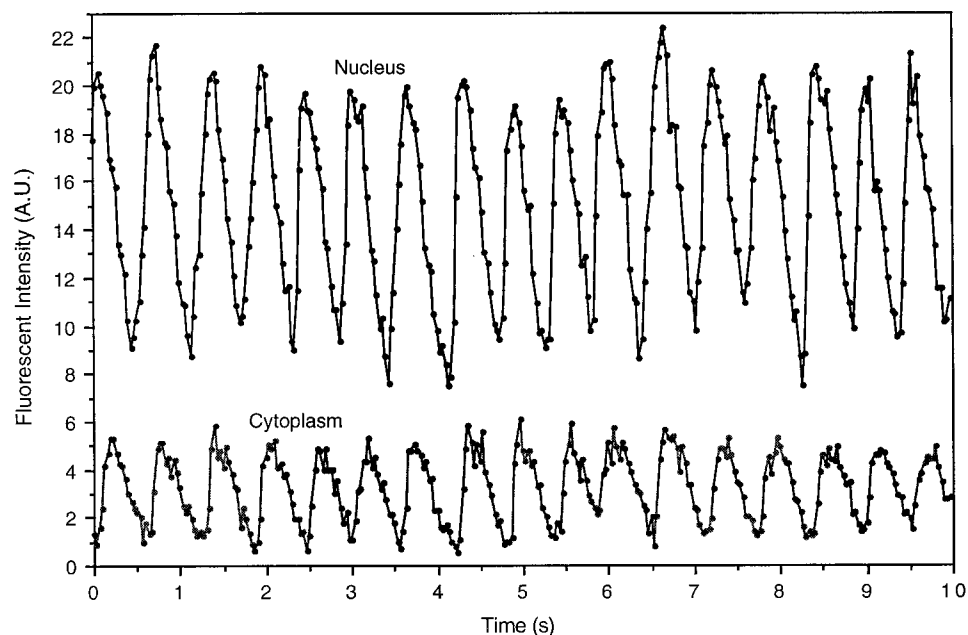


FIGURE 3 A video sequence of cultured cardiac myocytes showing the propagation of  $\text{Ca}^{2+}$  waves associated with cell beating. Frame 1 is the average of the rest of the frames to show the spatial relationship of cell A and B. In this particular video sequence, a delay of  $\sim 165$  ms (5 frames) is observed after the calcium wave in cell A reaches the border of cell B in frame 12 and before a stimulated calcium wave starts to form in cell B in frame 18. Time resolution = 33 ms. Scale bar, 10  $\mu\text{m}$ .

FIGURE 4 Measured fluo-3 fluorescent intensity in the nucleus and cytoplasm regions of a cardiac myocyte as a function of time. The beating frequency is  $\sim 1.7$  Hz. Time resolution,  $\sim 33$  ms.



Our design differs slightly in that only one mirror, instead of a roof-mirror pair, is used so that the incoming and returning beams form a slight angle (Fig. 1). This has the advantage of simpler optics and a smaller number of reflective surfaces. Also, the separation of the incoming and returning beams can be controlled by simply changing the orientation of the mirror. The amount of negative dispersion can be adjusted, as pointed out by Fork et al. (1984), by varying the separation of the prism pair, which we use for

coarse adjustment. In addition, we also move the second prism along its apex to control the amount of glass in the beam path as a fine adjustment, which proves to be effective. The criterion of the adjustment is to maximize the image intensity.

### Ratio-detection box

In the original design, fluorescent emission was descanned in the RCM 8000 by the same scan mirrors to achieve confocal detection. However, because of the high localization of two-photon excitation in the specimen, discussed above, such confocal detection is unnecessary with TPEM. Better detection efficiency is achieved without confocal optics. We have thus moved the detectors (PMTs) from the confocal port to the side port of the microscope, as illustrated in Fig. 1, and constructed a housing for the PMTs with two sets of dichroic mirrors and barrier filters for ratio imaging. This relocation of the detectors improves detection efficiency by reducing the number of reflection surfaces in the emission path and eliminating the confocal aperture in front of the PMTs.

The output from the two PMTs are formatted to NTSC signals, which can be displayed, processed, and recorded using standard video equipment. In addition to a videocassette recorder, the system currently uses a video optical memory disc recorder (OMDR), which is a higher quality recording medium and supports random access of individual video frames. Faster frame rates, at  $2\times$ ,  $4\times$ , and  $8\times$  the video rate, can be achieved with proportionally reduced scan lines per frame. For example, at  $4\times$  the video rate, which provides a time resolution of 8.3 ms, images can be digitized to  $512 \times 120$  pixels, and four images will be stored in one video frame.

### Specimen preparation

Cardiac myocytes were primary cultures from 1-day-old rats. Cells were examined 2–3 days after plating on glass-bottom culture dishes (from MatTek Corp., Ashland, MA). Stock solutions of fluo-3/AM (Minta et al., 1989), purchased from Molecular Probes (Eugene, OR), were made by dissolving  $50 \mu\text{g}$  of fluo-3/AM in  $50 \mu\text{l}$  of dimethylsulfoxide. Cells were washed three times with Hanks' balanced salt solution (HBSS) to remove the culture medium. A mixture of 1.5 ml of HBSS,  $7.5 \mu\text{l}$  of 20% Pluronic F-127, and  $10 \mu\text{l}$  of the fluo-3/AM stock solution was then added to the culture dishes. Cells were examined 0.5–1 h after loading the fluo-3.

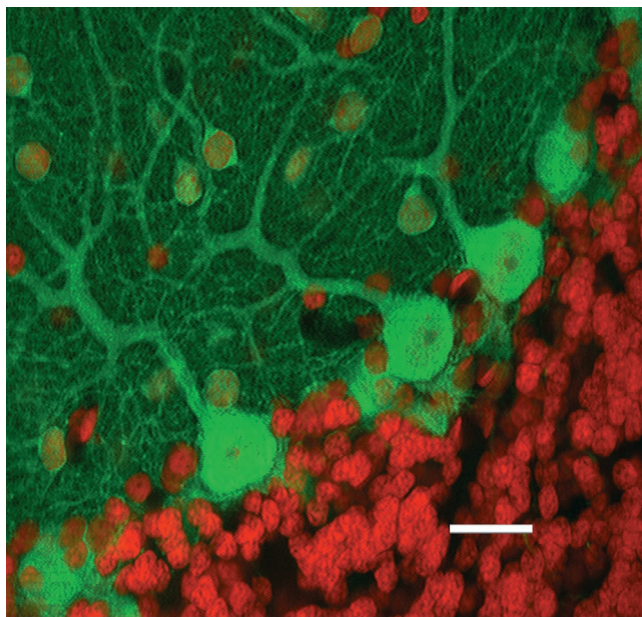


FIGURE 5 Two-photon excitation imaging of a fixed section of rat cerebellum. The Purkinje cells were stained with anti-parvalbumin-FITC (green) and DNA/RNA with propidium iodide (red). The image was formed by the dual emission of FITC and propidium iodide at 525 and 617 nm, respectively, with a single line excitation at 790 nm. Chroma filter set 31001 was used for imaging, which consists of a dichroic mirror (565DCLP) and two bandpass filters, D540/25 and D605/55, for the 525- and 617-nm emissions, respectively. Scale bar,  $10 \mu\text{m}$ .

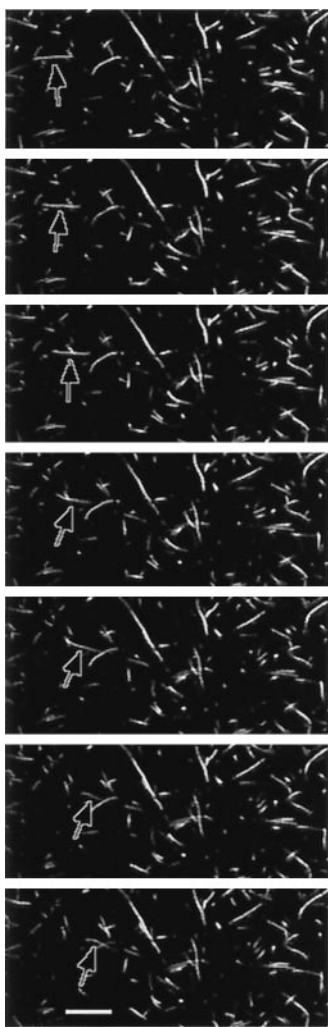


FIGURE 6 Images of *E. coli* expressing EGFP, selected from a video-rate sequence acquired with this TPEM. No averaging is performed. Arrows point to an *E. coli* string swimming at a speed of  $\sim 4.5 \mu\text{m/s}$ . Time separation between images is 0.5 s. Scale bar, 10  $\mu\text{m}$ .

Colonies of *Escherichia coli* JM109 (DE 3) strain transformed with EGFP gene in pRSETB (Invitrogen, San Diego, CA) were grown at room temperature and then suspended in 20 mM HEPES, pH 7.2, 100 mM KCl.

HeLa cells were imaged at room temperature in HBSS 2–5 days after transfection with yellow cameleon-2.1 cDNA using lipofectin (Gibco BRL, Gaithersburg, MD). Emission intensities at 480 and 535 nm were used for ratio imaging with Chroma filter set 31001 in the ratio detector box, which contained a dichroic mirror (505DCLP) and two band filters (D480/30 and D535/40) in front of the PMTs.

Yellow cameleon-3.1nu (nucleus) was constructed by extending the cDNA of yellow cameleon-3.1 by polymerase chain reaction at the 5' end with the sequence encoding the nuclear localization signal (MPKKKRKV). For simultaneous measurements of nuclear and cytosolic concentration of  $\text{Ca}^{2+}$ , HeLa cells were co-transfected with the cDNA of yellow cameleon-3.1 (1  $\mu\text{g}$ ) and -3.1nu (0.3  $\mu\text{g}$ ). Cells with similar fluorescent intensities from the nucleus and cytosol were chosen for ratio imaging.

## RESULTS AND DISCUSSION

The large separation of excitation and emission wavelength in a TPEM permits the effective removal of the excitation

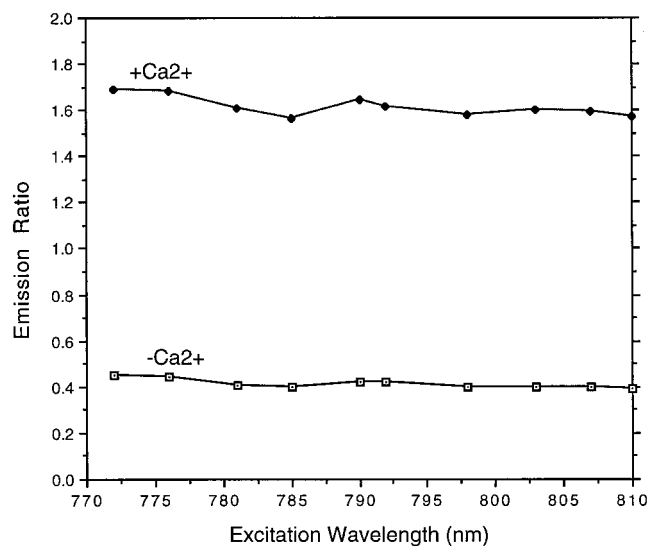


FIGURE 7 Emission ratio (535/480 nm) of the split yellow cameleon in vitro as function of two-photon excitation wavelength. The ratios are nearly constant in the wavelength range, being  $\sim 0.4$  for zero calcium level ( $-\text{Ca}^{2+}$ ) and 1.6 for saturating calcium level ( $\text{Ca}^{2+}$ ).  $\text{Ca}^{2+}$  causes a fourfold increase in emission ratio as a result of FRET in the split cameleon.

photons from the detection system. The use of the IR-cut filter in our system makes it safe to observe the fluorescent images through the microscope binocular eyepieces while the laser is scanning the specimen. The video-rate scanning makes it quite easy to observe the two-photon induced emission directly through the eyepieces. Transmitted light from a nonlaser source above the specimen can be blended in so that both the transmitted and fluorescent image can be viewed live through the binoculars, which proves to be helpful in finding and focusing the specimen.

With the use of the prechirper optics, which improves the temporal concentration of the laser pulses, the fluorescent emission is increased consistently by a factor of 1.75 over a wide range of laser power at the specimen. The modification and relocation of the ratio detectors from the confocal detection arrangement to the side port of the microscope to form a nonconfocal detection configuration boosted the detection efficiency by a factor of 2.25. So an overall improvement by a factor of nearly 4-fold was achieved in detected signal with the same laser power at the specimen.

As the RCM 8000 microscope was originally designed for UV to blue light excitation, IR power throughput is far from optimum. With a 40 $\times$  water objective lens, the overall IR power throughput goes down linearly with wavelength from 9% at 772 nm to 4.3% at 810 nm. Most power loss takes place at the beam expander (Fig. 1) where the laser beam goes through a small aperture before being expanded to over-fill the back-focal plane of the objective lens. The maximal IR power routinely achievable at the specimen is  $\sim 65 \text{ mW}$ , and the data presented in this paper are collected with a laser power of  $\sim 20 \text{ mW}$  at the specimen unless indicated otherwise. This power level is well below satura-

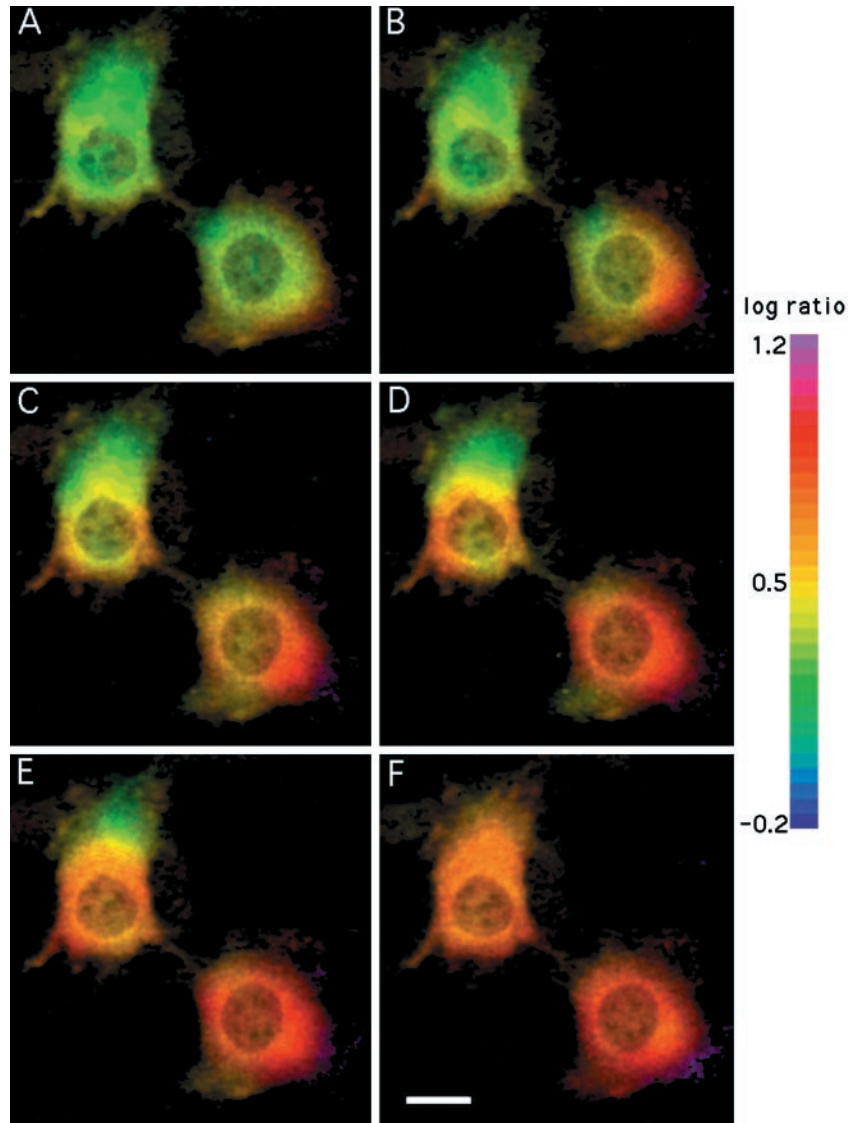


FIGURE 8 Ratio imaging (535/480 nm) of calcium wave in HeLa cells expressing yellow cameleon-2.1 without targeting signals. The calcium wave (red), which was created with the application of 0.1 mM histamine, which triggers  $\text{Ca}^{2+}$  release in the cells, can be seen to propagate across each cell. Images A and F were recorded 1 s before and 6 s after the application of histamine, respectively. Time separation between images B–E is 132 ms. Scale bar, 10  $\mu\text{m}$ .

tion as the power-square dependency still holds, and at this power level specimens can be observed for minutes under continuous illumination without appreciable drop in emission with the cameleons. Although the IR power throughput of the system clearly needs to be improved, it is not a limiting factor at the present time. As stated earlier, the laser power at the specimen is controlled by turning a partially reflective wheel that has a gradually varying reflectivity.

Fig. 3 shows a video sequence taken at 30 frames/s of cultured cardiac myocytes of a 1-day-old rat. The cells were loaded with fluo-3, a  $\text{Ca}^{2+}$  indicator dye, as described previously. The  $\text{Ca}^{2+}$  waves, representing the periodic activities of the cells, can be seen propagating in the cells. This propagation is often, but not always, accompanied by visible motion of the cells. In this particular sequence, the  $\text{Ca}^{2+}$  wave in cell A appears to be coupled to the  $\text{Ca}^{2+}$  wave in its neighbor, cell B. Fig. 4 gives the intensity measurements in the nucleus and cytoplasm regions of a cell in a similar video sequence and clearly reveals a beating rate of

$\sim 1.7$  Hz. In addition, some irregularities in the beating, both in frequency and intensity, are evident in the measurement.

For fixed specimens for which time resolution is not an important concern, up to 128 video frames (4.3 s) from each of the two signal channels can be averaged simultaneously on-line to increase signal-to-noise ratio. Fig. 5 gives an example image of a fixed section of rat cerebellum in which Purkinje cells were stained with fluorescein isothiocyanate (FITC)-conjugated anti-parvalbumin (green) and DNA/RNA with propidium iodide (red). A single line (790 nm) was used to excite both the FITC and propidium iodide fluorophores, which emit at 525 and 617 nm, respectively.

The green fluorescent protein (GFP) and its derivatives are important cell biological markers of cell morphology and protein trafficking. GFPs have been genetically modified to emit, for example, in yellow (YFPs) and cyan (CFPs), and the efficiency of their chromophore folding at 37° has been enhanced as well, resulting in enhanced GFPs (EGFPs), which are ideal for video-rate imaging due to their

high brightness. Fig. 6 presents a video sequence of *E. coli* expressing EGFPs. One bacterial string is seen to swim at a speed of  $\sim 4.5 \mu\text{m/s}$ . The high brightness of the EGFPs allows useful images to be recorded at video rate with a minimal laser power of  $\sim 2.7 \text{ mW}$  at the specimen.

GFPs can not only reveal cell and protein movements but can also be engineered into FRET-based emission-ratioing indicators of biochemical signals such as fast  $\text{Ca}^{2+}$  transients. To see whether such indicators are suitable for TPTEM, in vitro samples known to give large emission ratio changes in a conventional spectrofluorometer were tested on the microscope. ECFP-CaM (enhanced cyan fluorescent protein fused to *Xenopus* calmodulin) and M13-EYFP (calmodulin-binding peptide fused to enhanced yellow fluorescent protein) reversibly associate in a  $\text{Ca}^{2+}$ -dependent manner (Miyawaki et al., 1997). This unfused pair of proteins shows a particularly large  $\text{Ca}^{2+}$ -induced change in FRET because they come together from an effectively infinite distance, whereas their dynamic range is reduced when genetically fused because they already show significant FRET before addition of  $\text{Ca}^{2+}$ . We measured the YFP and CFP emissions from equimolar mixtures of ECFP-CaM and M13-EYFP at zero and saturating  $\text{Ca}^{2+}$  as a function of TPTEM excitation wavelength. Although the emission intensity at both wavelengths varied considerably with the excitation wavelength, the ratio of 535- to 480-nm emissions remained reasonably constant, being  $\sim 0.4$  and  $1.6$  for zero and saturating  $\text{Ca}^{2+}$  levels, respectively (Fig. 7). A fourfold change in the emission ratio was therefore obtained in the excitation wavelength range of 770–810 nm. For comparison, the 534:480-nm emission ratios in a conventional spectrofluorometer with one-photon excitation were 0.584 and 2.11 at zero and saturating  $\text{Ca}^{2+}$ , respectively, a 3.62-fold change in emission ratio. These results demonstrate that two-photon excitation in the wavelength range of 770–810 nm can selectively excite CFP. Thus, the CFP-YFP pairs can be used for  $\text{Ca}^{2+}$  imaging and, more generally, for imaging of protein-protein interactions in TPTEM.

Our currently preferred indicators for intracellular  $\text{Ca}^{2+}$  measurements are “yellow cameleons” 2.1 and 3.1 (A. Miyawaki and R. Y. Tsien, submitted for publication). These proteins, like their predecessors yellow cameleon 2 and 3, consist of ECFP-CaM fused to M13-EYFP via a Gly-Gly spacer (Miyawaki et al., 1997). The 2 and 2.1 versions contain wild-type calmodulin, whereas the 3 and 3.1 versions have a somewhat reduced  $\text{Ca}^{2+}$  affinity and a simpler binding curve due to mutation of Glu104 to Gln within one of the  $\text{Ca}^{2+}$ -binding sites of calmodulin. Versions 2.1 and 3.1 have reduced sensitivity to pH interference because Val68 and Gln69 within EYFP were mutated to Leu and Lys, respectively (A. Miyawaki and R. Y. Tsien, submitted). When yellow cameleon-2.1 was expressed in HeLa cells without any targeting signals, the fluorescence was uniformly distributed in the cytoplasm but excluded from the nucleus (Fig. 8). With application of 0.1 mM histamine, which triggers  $\text{Ca}^{2+}$  release in the cells, we were able to observe and record a  $\text{Ca}^{2+}$  wave with a good time

resolution of 67 ms with two-frame averaging. In the video sequence in Fig. 8, the  $\text{Ca}^{2+}$  wave can be seen to propagate across each cell with a slightly different latency. The time for the ratio to rise from 10% to 90% of the maximum in the HeLa cells was  $\sim 0.4 \text{ s}$  as measured from the time course (Fig. 9) for the cytoplasmic regions of the cells in Fig. 8.

It has been controversial whether nuclear  $\text{Ca}^{2+}$  concentration is regulated independently of the cytosolic  $\text{Ca}^{2+}$  concentration (Malviya and Rogue, 1998). Comparative measurements of nuclear and cytosolic  $\text{Ca}^{2+}$  concentration have been performed using synthetic fluorescent chelators (Al-Mohanna et al., 1994; Brown et al., 1997; Malviya and Rogue, 1998). However, the cytosolic signal is often contaminated by that from intracellular organelles, such as the endoplasmic reticulum, into which the chelators can be compartmentalized. The  $\text{Ca}^{2+}$ -sensitive photoprotein aequorin has been localized specifically in nucleus and cytosol (Brini et al., 1994, 1998; Badminton et al., 1996, 1998), but it has not been possible to image nuclear and cytosolic aequorin signals simultaneously in the same individual cells. We have expressed yellow cameleon-3.1 simultaneously in the nucleus and cytosol by mixing two cDNAs, one encoding a cytosolic protein without targeting signals, the other encoding the same protein with a nuclear targeting sequence from SV40. We controlled the relative amount of the two cDNAs to balance the indicator's concentration between the two compartments. TPTEM ratio images of two HeLa cells 2 s before and after the application of 0.1 mM histamine are shown in Fig. 10, and Fig. 11 gives the time course measurement of emission ratio in the nucleus and cytoplasm when histamine, cyproheptadine, ionomycin, and  $\text{CaCl}_2$  are applied, in that order, to the HeLa cells. No obvious  $\text{Ca}^{2+}$  concentration gradient across the nuclear membrane is evident in the images in Fig. 10 or higher time-resolution video sequences (data not shown).

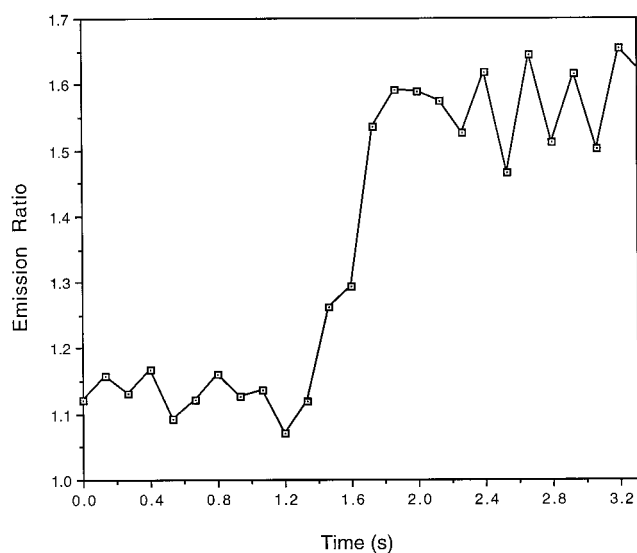


FIGURE 9 Time course of average  $\text{Ca}^{2+}$  in HeLa cells associated the application of histamine, measured from the cytoplasm region of cells in Fig. 8. The rise time is  $\sim 0.4 \text{ s}$ .

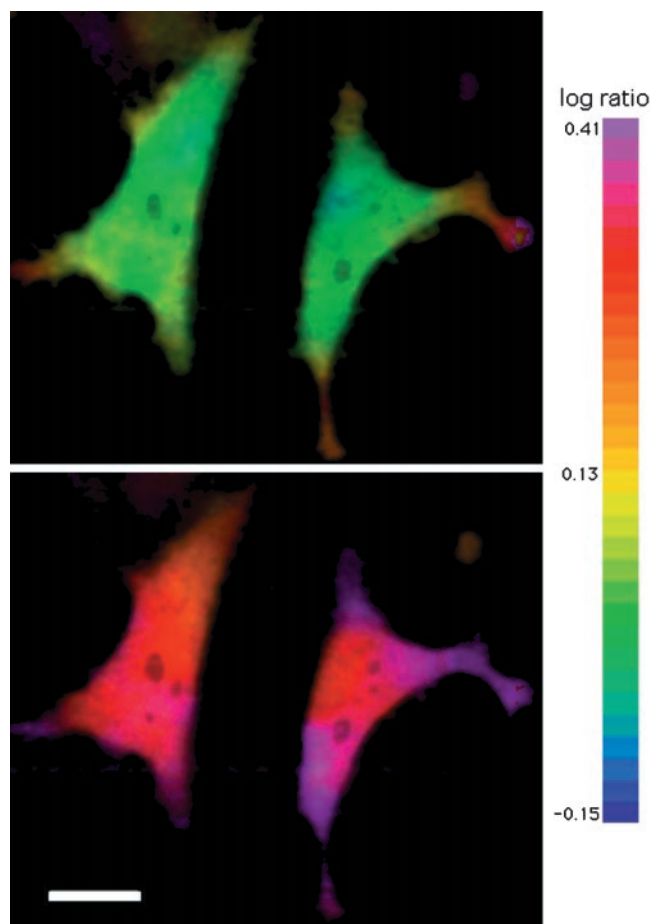


FIGURE 10  $\text{Ca}^{2+}$  ratio images (535/480 nm) of HeLa cells expressing yellow cameleon-3.1 and -3.1nu, recorded 2 s before (A) and after (B) the application of 0.1 mM histamine.

## CONCLUSIONS

Video-rate scanning two-photon excitation fluorescent microscopy can be performed routinely with an average laser power of  $\sim 20$  mW at the specimen with the commonly used fluorescent dyes and as low as 2.7 mW with some fluorophores such as enhanced GFP (EGFP) in bacteria. Aside from the many known advantages of TPEM over conventional one-photon excitation as discussed in the Introduction, we also showed that 1) elimination of confocal optics significantly improves detection efficiency by a factor of 2.25 in our case and 2) TPEM conveniently and selectively excites CFP-YFP pairs for imaging protein-protein interaction and  $\text{Ca}^{2+}$  levels via FRET. One-photon excitation would require wavelengths of 430–440 nm, which are not available from the argon or krypton lasers most commonly found on confocal microscopes, although helium-cadmium lasers could perhaps be substituted. The tunable Ti:sapphire laser is a near-universal replacement in TPEM for all these separate one-photon excitation sources. Genetically encoded indicators and TPEM are mutually complementary in that viral or transgenic delivery in principle solves the problem of introducing the probes deep inside intact tissues

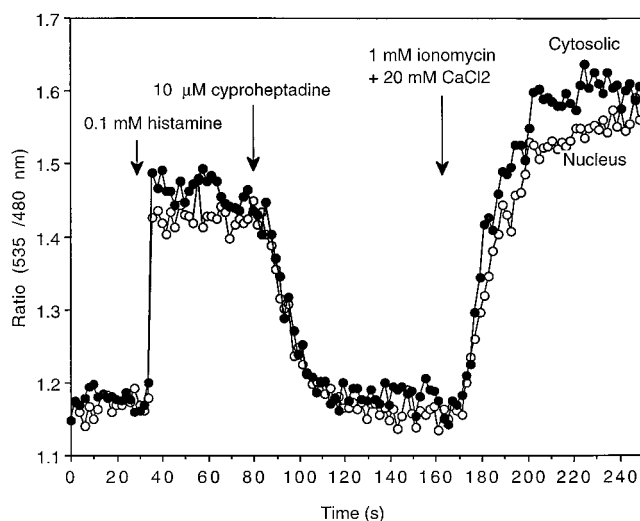


FIGURE 11 Time course of nuclear and cytosolic concentration of  $\text{Ca}^{2+}$  in HeLa cells when histamine, cyproheptadine, ionomycin, and  $\text{CaCl}_2$  are applied in sequence.

or organisms, whereas TPEM offers the best prospect of optical imaging at such depths. Compared with wide-field imaging followed by off-line computational removal of out-of-focus information, TPEM now has the advantages of on-line imaging at video rate or faster and the ability to acquire perfectly registered, simultaneous images at two or more emission wavelengths, which is crucial for FRET indicators. Video-rate imaging will be particularly essential for visualizing inter- or intracellular dynamics in excitable or motile cells or when multiple planes of focus need to be monitored nearly simultaneously. Compared with the line-excitation mode and rotating microlens array approaches, which provide very fast scan rates, our implementation does not require spatial discrimination between the fluorescent photons and should therefore be superior in the case of scattering specimens where whole-field detection, as provided by PMTs, leads to an increased collection efficiency. Point scanning also means that multiple emission channels can be simultaneously and cheaply collected with perfect registration.

We thank John Adams for providing the cardiac myocyte cultures, Jeffrey Squier for discussions on the prechirper optics, and Tom Deerinck and John Crum for their assistance.

This work was supported by National Institutes of Health grants RR-04050 and NS-14718, National Science Foundation grant DMR 96-12252, and a research grant from Nikon Corp. to M.H. Ellisman, and grant NS-27177 and an HHMI Investigatorship to R.Y. Tsien.

## REFERENCES

- Alfrey, A. J. 1989. Modeling of longitudinally pumped CW Ti:sapphire laser oscillators. *IEEE J. Quantum Electronics*. 25:760–766.
- Al-Mohanna, F. A., K. W. T. Caddy, and S. R. Bolsover. 1994. The nucleus is insulated from large cytosolic calcium ion changes. *Nature*. 367:745–750.

- Amos, W. B., J. G. White, and M. Fordham. 1987. Use of confocal imaging in the study of biological structures. *Appl. Optics*. 26:3239–3243.
- Åslund, N., A. Liljeborg, P.-O. Forsgren, and S. Wahlsten. 1998. Three dimensional digital microscopy using the PHOIBOS scanner. *Scanning*. 9:227–235.
- Badminton, M. N., A. K. Campbell, and C. M. Rembold. 1996. Differential regulation of nuclear and cytosolic  $\text{Ca}^{2+}$  in HeLa cells. *J. Biol. Chem.* 271:31210–31214.
- Badminton, M. N., J. M. Kendal, C. M. Rembold, and A. K. Campbell. 1998. Current evidence suggests independent regulation of nuclear calcium. *Cell Calcium*. 23:79–86.
- Berge, R. R. 1979. A theoretical analysis of the two-photon properties of linear polyenes and the visual chromophores. *J. Chem. Phys.* 70:165.
- Bewersdorf, J., R. Pick, and S. W. Hell. 1998. Multifocal multiphoton microscopy. *Optics Lett.* 23:655–657.
- Brakenhoff, G. J., M. Muller, and J. Squier. 1995. Femtosecond pulse width control in microscopy by two-photon absorption autocorrelation. *J. Microsc.* 179:253–260.
- Brakenhoff, G. J., J. Squier, T. Norris, A. C. Bliton, M. H. Wade, and B. Athey. 1996. Real-time two-photon confocal microscopy using a femtosecond, amplified Ti:sapphire system. *J. Microsc.* 181:253–259.
- Brini, M., R. Marsault, C. Bastianutto, T. Pozzan, and R. Rizzuto. 1994. Nuclear targeting of aequorin: a new approach for measuring nuclear  $\text{Ca}^{2+}$  concentration in intact cells. *Cell Calcium*. 16:259–268.
- Brini, M., M. Murgia, M. Pasti, D. Picard, T. Pozzan, and R. Rizzuto. 1998. Nuclear  $\text{Ca}^{2+}$  concentration measured with specifically targeted recombinant aequorin. *EMBO J.* 12:4813–4819.
- Brown, G. R., M. Kohler, and P. Berggren. 1997. Parallel changes in nuclear and cytosolic calcium in mouse pancreatic  $\beta$ -cells. *Biochem. J.* 325:771–778.
- Carlsson, K., P. Danielsson, R. Lenz, A. Liljeborg, L. Majlof, and N. Åslund. 1985. Three-dimensional microscopy using a confocal laser scanning microscope. *Optics Lett.* 10:53–55.
- Curley, P. F., A. I. Ferguson, J. G. White, and W. B. Amos. 1992. Application of a femtosecond self-sustaining mode-locked Ti:sapphire laser to the field of laser scanning confocal microscopy. *Optics Quantum Electronics*. 24:851–895.
- Denk, W., J. H. Strickler, and W. W. Webb. 1990. Two-photon laser scanning fluorescence microscopy. *Science*. 26:73–76.
- Denk, W., and K. Svoboda. 1997. Photon upmanship: why multiphoton imaging is more than a gimmick. *Neuron*. 18:351–357.
- Fork, R. L., O. E. Martinez, and J. P. Gordon. 1984. Negative dispersion using pairs of prisms. *Optics Lett.* 1282:–7786–7711.
- Guild, J. B., C. Xu, and W. W. Webb. 1997. Measurement of group delay dispersion of high numerical aperture objective lenses using two-photon excited fluorescence. *Appl. Optics*. 36:397–401.
- Loudon, R. 1983. *The Quantum Theory of Light*, 2nd ed. Oxford University Press, London. 334–384.
- Malviya, A. N., and P. J. Rague. 1998. “Tell me where is calcium bred”: clarifying the roles of nuclear calcium. *Cell*. 92:17–23.
- Minta, A., J. P. Y. Kao, and R. Y. Tsien. 1989. Fluorescent indicators for cytosolic calcium based on rhodamine and fluorescein chromophores. *J. Biol. Chem.* 264:8171–8178.
- Miyawaki, A., J. Llopis, R. Heim, J. M. McCaffery, J. A. Adams, M. Ikura, and R. Y. Tsien. 1997. Fluorescent indicators for  $\text{Ca}^{2+}$  based on green fluorescent proteins and calmodulin. *Nature*. 388:882–887.
- Piston, D. W., B. D. Bennett, and G. Ying. 1995. Imaging of cellular dynamics by two-photon excitation microscopy. *J. Microsc. Soc. Am.* 1:25–34.
- Tsien, R. Y., and B. J. Bacskai. 1995. Video-rate confocal microscopy. *In Handbook of Biological Confocal Microscopy*. J. B. Pawley, editor. Plenum press, New York. 459–478.
- White, J. G., W. B. Amos, and M. Fordham. 1987. An evaluation of confocal versus conventional imaging of biological structures by fluorescence light microscopy. *J. Cell Biol.* 105:41–48.
- Xu, C., and W. W. Webb. 1996. Measurement of two-photon excitation cross sections of molecular fluorophores with data from 690 to 1050 nm. *J. Optics Soc. Am. B.* 13:481–491.
- Xu, C., W. Zipfel, J. B. Shear, R. M. Williams, and W. W. Webb. 1996. Multiphoton fluorescence excitation: new spectral windows for biological nonlinear microscopy. *Proc. Natl. Acad. Sci. U.S.A.* 93: 10763–10768.